Alexandria Engineering Journal (2023) 64, 847–858

HOSTED BY

ELSEVIER

Alexandria University

Alexandria Engineering Journal

www.elsevier.com/locate/aej
www.sciencedirect.com

Study the effect of changing Cables' pattern on the workspace of a six DOF floating parallel marine robot (FPMR)

Mamon M. Horoub [a,*], **Ayman M.A. Horoub** [b], **Sikandar Khan** [c], **Ahmad Albalasie** [a], **Sajid Ali** [d], **Ihab Abu Ajamieh** [a], **Ammar Alzaydi** [c]

[a] *Department of Mechanical and Mechatronics Engineering, Birzeit University, Birzeit, Palestine*
[b] *Mathematics Department, Hebron University, Hebron, Palestine*
[c] *Department of Mechanical Engineering, King Fahd University of Petroleum and Minerals, Dhahran, Saudi Arabia*
[d] *Mechanical and Energy Engineering Department, Imam Abdulrahman bin Faisal University, Saudi Arabia*

Received 18 November 2021; revised 21 July 2022; accepted 25 August 2022
Available online 06 September 2022

KEYWORDS

Dynamic response;
Workspace;
Floating Parallel Marine Robot;
Stewart-Gough parallel manipulator;
6–6 and 6–3-3 FPMR

Abstract In this study, a Floating Parallel Marine Robot (FPMR) is studied while it is subjected to external forces generated by the sea waves. Two FPMR cable-bundles' configurations are used. The 6–6 Stewart-Gough parallel manipulator configuration is compared with a new cable-bundles' configuration called 6–3-3 FPMR. The effect of changing cable-bundles' configuration is explored to enhance the workspace and the dynamic behavior of the FPMR. This study is performed using six DOFs FPMR having twelve cables i.e. 6 bundles. Over the FPMR workspace, the dynamic response and platform stiffness are investigated. The workspace and the dynamic analysis of FPMR are enhanced using the new 6–3-3 cable-bundles' configuration.

1. Introduction

Cable-Driven Parallel Robots (CDPRs) are robots with high acceleration capability and a large workspace. Cables/Cords are used as a replacement for rigid links to move the floating structure of the CDPR. CDPR is used for many purposes such as rescue efforts, disasters search, and managing dangerous substances [1]. Furthermore, it is utilized in sports/theater/entertainment areas/fields and telescope radio stations. Different CDRP designs are analyzed e.g. NIST Robocrane [2], Falcon-7 [3], WARP [4], WiRo [5], DeltaBot [6], and the hybrid cable-actuated robot [7].

Cable-driven parallel platforms have two main parts, a floating structure, and a cable system. Designing the cable

* Corresponding author.
E-mail addresses: mhoroub@birzeit.edu (M.M. Horoub), aymanh@hebron.edu (A.M.A. Horoub), sikandarkhan@kfupm.edu.sa (S. Khan), abalasie@birzeit.edu (A. Albalasie), sakzada@iau.edu.sa (S. Ali), iabuajamieh@birzeit.edu (I. Abu Ajamieh), ammar.alzaydi@kfupm.edu.sa (A. Alzaydi).

Peer review under responsibility of Faculty of Engineering, Alexandria University.

https://doi.org/10.1016/j.aej.2022.08.043
1110-0168

system is critical due to its effectiveness in controlling the floating structure part. For further enhancement, several factors should be considered when designing the cable system, such as the distribution scheme of the wire tension, cables' pretension, cables' lengths, cables' weight, cables' elasticity, cost-effectiveness, and other material properties [8–14]. The cables' configuration is an additional aspect that could be studied and analyzed to have a better workspace and dynamic behavior. A few studies have discussed the impact of the cables' configuration on the working of the floating structure marine platforms [15–19]. Alternatively, several non-floating robotic studies have used cables to explore the dynamic response and the workspace of CDPRs [20–29]. CDPRs can be used in the marine environment for different purposes such as oil/gas exploration [19,30,31].

A thorough study based on Horoub *et al.* analysis [19,32], is performed to investigate the impact of marine environments on the performance of CDPR. Since the performance of the FPMR is controlled by cables' locations/positions [19], this study intends to examine the impact of two dissimilar cables' configurations on the workspace and the dynamic behavior of FPMR. The proposed arrangement of cables in this study is inspired by the common 6x6 Stewart-Gough platform, a well-known concept in the field of parallel robots [33]. The new cables' configuration (6–3-3) is explored and compared with the conventional (6–6) Stewart-Gough parallel robot configuration. The dynamic performance, the tension of the cables, and stiffness of the platform are examined across the FPMR workspace i.e., the work effective area on the sea surface.

The general layout of the FPMR is presented in Fig. 1. This layout consists of six cable bundles, each one represents two cables. Each cable bundle is driven by one motor that is installed on the FPMR floating structure. The total tension/stiffness of each cable-bundle is the summation of the tension/stiffness of the two cables at that cable bundle.

Unresolved technical challenges in the field of underwater robot manipulators and floating platforms make the experimental validation of the proposed algorithm a difficult task. Some of these challenges one might face in the experimental implementation are (i) Lack of Global Navigation Satellite Systems (GNSS), and under-water sensing devices [34]. (ii) the requirements of acoustic-based communication and motion control necessitate a high degree of reliability. (iii) Harsh underwater conditions such as, high pressures and low temperatures that require the design and the availability of water-tight equipment and devices. (iv) Availability of non-conventional technologies such as biological batteries and fuel cells which are often used as a power source in underwater experiments [35].

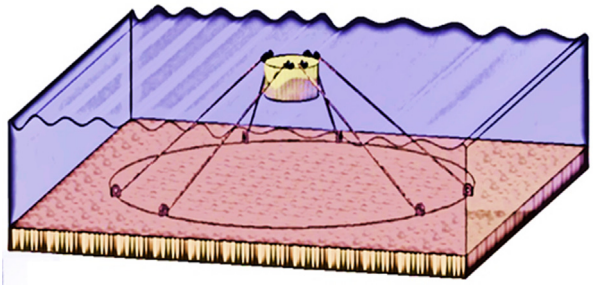

Fig. 1 General Layout of the FPMR.

It is necessary to clarify that the cables' configuration (6–3) [36] is widely used in some robotics applications, however, and based on the authors' knowledge, the new proposed configuration (6–3-3) isn't used before in such cable-bundles' configuration can be rearranged to have a better configuration that enhances the FPMR performance and the functioning of the system. This yields to minimize the possibility of having cable-bundles' compression which leads to system failure. Hence, one of the aspects that can be used to have an effective FPMR configuration is to adjust the vertical altitude of the locations of some of the cable-bundles on the FPMR floating structure. In the case of the new configuration (6–3-3 FPMR), three out of the six cable-bundles are attached to the bottom side of the floating structure, while the others are attached to the top side of the 6–3-3 FPMR floating structure. The novelty of this study is the utilization of the new proposed configuration (6–3-3) in FPMR and evaluate its performance to compare the results with the (6–6) Stewart-Gough parallel robot configuration and present the benefits of using the new configuration (6–3-3). Below are the main issues that have been discussed:

- The impact of two dissimilar cable-bundles' configurations on the workspace, cable-bundles tensions, and the dynamic behavior of FPMR.
- The influence of the hydrostatic effect on the dynamic response of FPMR.
- The modified cable-bundles configuration that is used to improve the stiffness and cable-bundle tensions, increase the workspace, and enhanced the performance of FPMR.

This paper is organized as follows: FPMR layout is presented in section 2. Section 3 introduces the dynamic analysis of the system. While section 4 presents the methodology used in the current study. In addition, section 5 presents and evaluates the performance of FPMR with the (6–3-3) configuration and it compares with (6–6). Finally, the paper conclusion presented in section 6.

2. FPMR layout

FPMR is exposed to the sea waves' forces that are instigated by climatic factors. The current work is following the studies performed by Horoub *et al.* and Finnegan *et al.* [19,37]. The mathematical equations that represent the excitation forces of the seawater waves on a circular floating structure (shown in Fig. 2) were discussed in detail [19,37] and available in Appendix A.

The proposed setup of the FPRM floating structure and the sea waves parameters are listed in Table 1. These parameters were utilized in finding the excitation forces in the six DOFs directions, which are the surge, heave, and pitch. Fig. 2 presents an example of the sea waves' excitation forces using those parameters.

In Fig. 3, two layouts of the FPMR are shown. The six cable-bundles are attached to the seabed by anchors placed along the perimeter of a 200 m radius circle. These anchors are located at points A_1, A_2, A_3, A_4, A_5, and A_6. Those points have angles, of 15, 45, 135, 165, 255, and 285 degrees with

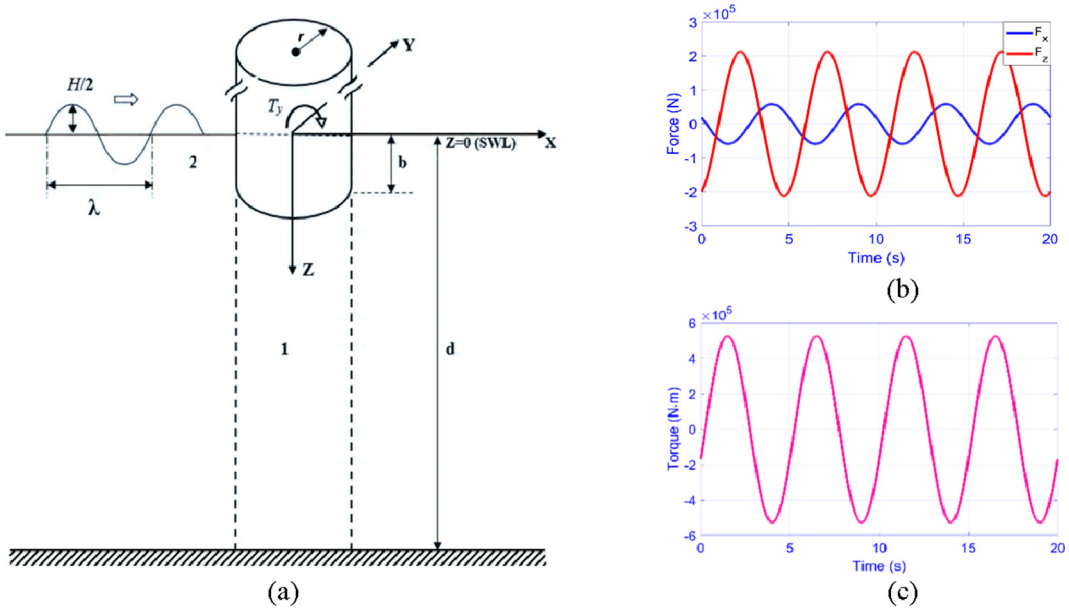

Fig. 2 Sea waves' excitation forces. (a) Water waves are subjected to a circular floating structure. (b) Forces surge, heave direction. (c) Torque in the pitch direction.

Table 1 The major parameters of the FPMR floating structure and the sea wave. b_w is the submerge depth due to FPMR weight.

Parameter	Definition	Value
r	The floating structure radius	5 m
d	Water depth is considered in this study. The distance between the base and the platform	50 m
k_o	The wave number of the sea wave	0.16095 m^{-1}
H	Wave amplitude peak to peak	1 m
ρ_f	Water Density	1000 $\frac{kg}{m^3}$
b_w	The submerge depth due to FPMR weight	0.6 m
g	Gravitational acceleration	9.81 $\frac{kg}{m^3}$
b	Total submerged depth of the floating structure ($b_w$is included)	–
SWL	Sea water level	–

respect to the positive x-axis. Six motors, located on the floating structure (circular disc with a 5 m radius) are used to drive the six cable-bundles. The motors are located at points B_1, B_2, B_3, B_4, B_5, and B_6. Those points have angles of 345, 75, 105, 195, 225, and 315 with respect to the positive x-axis.

The difference between the two layouts is shown in Fig. 3. In the case of the new configuration (6–3-3 FPMR), three out of the six cable-bundles (B_1, B_3, B_5) are attached to the bottom side of the 6–3-3 FPMR floating structure. While the other cable-bundles (B_2, B_4, B_6) are attached to the top side.

3. Dynamic analysis

The dynamic analysis of the FPMR is performed using the modal analysis technique. The FPMR is studied considering the concepts of the rigid body dynamics. Thus, around an equilibrium position, the equation of motion for FPMR is:

$$\boldsymbol{M}(\boldsymbol{X})\ddot{\boldsymbol{X}} + \boldsymbol{C}(\boldsymbol{X})\dot{\boldsymbol{X}} + \boldsymbol{K}(\boldsymbol{X})\boldsymbol{X} = \boldsymbol{F}(t, \boldsymbol{X}) \tag{1}$$

where $\boldsymbol{M}(\boldsymbol{X})$ is the FPMR mass matrix, $\boldsymbol{X} = [\, x \quad y \quad z \quad \psi \quad \theta \quad \varphi \,]^T$ is the displacement vector where the inside entries represent the surge, sway, heave translation motions and the roll, pitch, and yaw rotation angles, $\boldsymbol{C}(\boldsymbol{X})$ is the FPMR damping matrix, $\boldsymbol{K}(\boldsymbol{X})$ is the FPMR stiffness matrix, and $\boldsymbol{F}(t, \boldsymbol{X})$ represents the external forces and moments. To examine the FPMR dynamics, the stiffness and the mass matrices should be calculated. The main objective of this work is to study the effect of changing cable-bundles' configuration to enhance the workspace, hence and for more simplicity, the effect of the damping matrix is not considered in the model.

There are two inertial components of the FPMR mass matrix. The first one is the structural-mass matrix ($\boldsymbol{M_s}$) and the second one is the added-mass matrix ($\boldsymbol{M_a}$) (hydrodynamic mass matrix). The mass matrix of the FPMR is shown in Eq. (2).

$$\begin{aligned} M &= M_s + M_a \\ &= \begin{bmatrix} m & 0 & 0 & 0 & 0 & 0 \\ 0 & m & 0 & 0 & 0 & 0 \\ 0 & 0 & m & 0 & 0 & 0 \\ 0 & 0 & 0 & I_{44} & 0 & 0 \\ 0 & 0 & 0 & 0 & I_{55} & 0 \\ 0 & 0 & 0 & 0 & 0 & I_{66} \end{bmatrix} \\ &+ \begin{bmatrix} m_{a11} & 0 & 0 & 0 & m_{a15} & 0 \\ 0 & m_{a11} & 0 & m_{a15} & 0 & 0 \\ 0 & 0 & m_{a33} & 0 & 0 & 0 \\ 0 & m_{a15} & 0 & m_{a44} & 0 & 0 \\ m_{a15} & 0 & 0 & 0 & m_{a44} & 0 \\ 0 & 0 & 0 & 0 & 0 & 0 \end{bmatrix} \end{aligned} \tag{2}$$

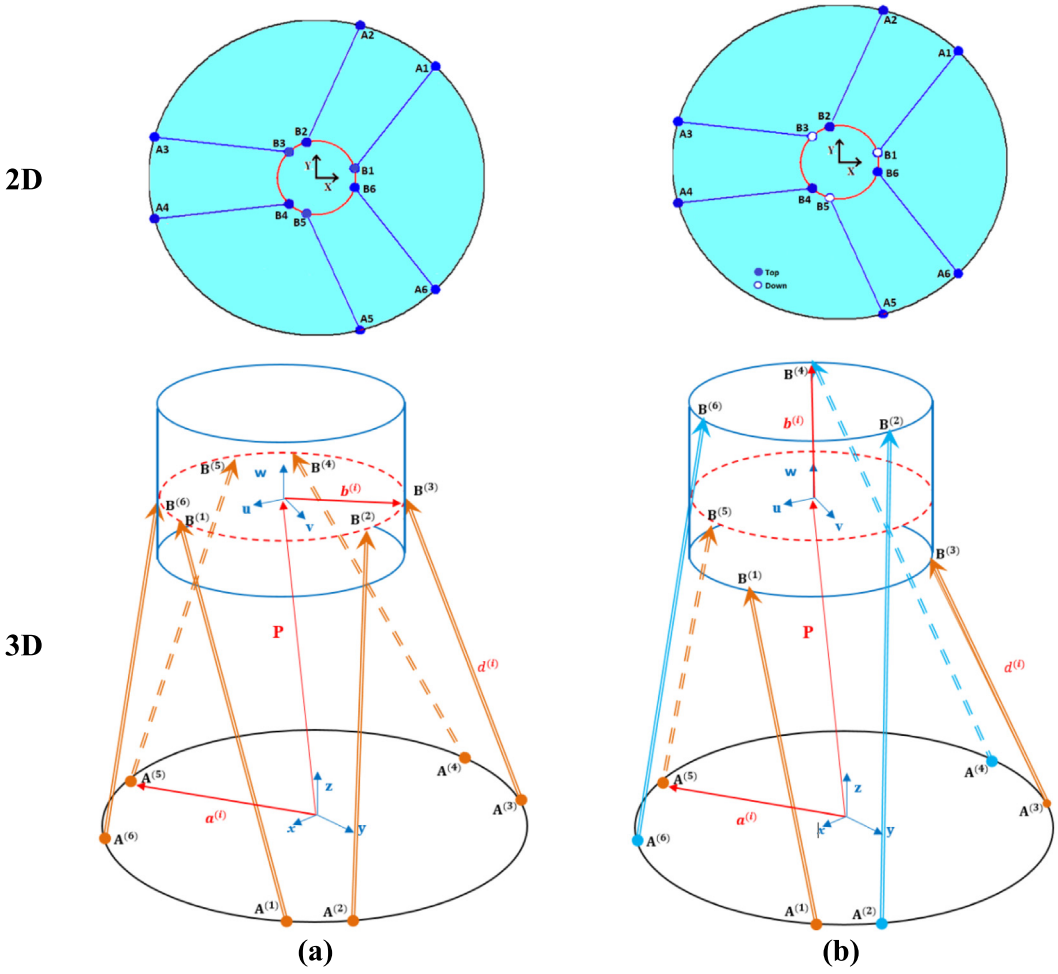

Fig. 3 FPMR configuration. (a) 6–6 configuration. (b) 6–3-3 configuration.

where the subscripts 1, 2…, 6 refer to the six DOFs. $m = \pi\rho_f br^2$ is the floating structure mass, $I_{44} = I_{55} = \frac{1}{12}m\left(3r^2 + h^2\right)$, $I_{66} = \frac{1}{2}mr^2$; $m_{a11} = \pi C_a\rho_f r^2 b$; $m_{a33} = \frac{4}{3}\rho_f r^3$; $m_{a51} = m_{a15} = \pi C_a\rho_f r^2 b\left(\bar{KG} + b/2\right)$; and $m_{a55} = \pi C_a\rho_f r^2\left(\frac{b^3}{3} + \bar{KG}^2 + \bar{KG}\,b^2\right)$; $\bar{KG}$ represents the distance between the center of gravity (C_g) and the Still Water Level (SWL), r is the floating structure radius, h is the floating structure height,C_a represents the added mass coefficient, and ρ_f is the water density. Any difference in the cable-bundles' weight and the floating structure's weight are indirectly compensated using the submerged depth (b) that affects the cable-bundles tensions as shown in Fig. 4.

Cable-bundles stiffness depends on the type of cable-bundles material, cable-bundles pre-tension and the magnitude of applied axial tension depend on the position and orientation of the floating structure. There are three stiffness matrices for the FPMR. The first one is due to the effect of the strengths of the cable-bundles ($\boldsymbol{K}_k$), the second one is due to the effect of the tensions between the cable-bundles ($\boldsymbol{K}_\tau$) and the third one is the hydrostatic stiffness matrix ($\boldsymbol{K}_a$).

Behzadipour and Khajepour work [29] has been followed to find the first two parts of the FPMR stiffness matrix.

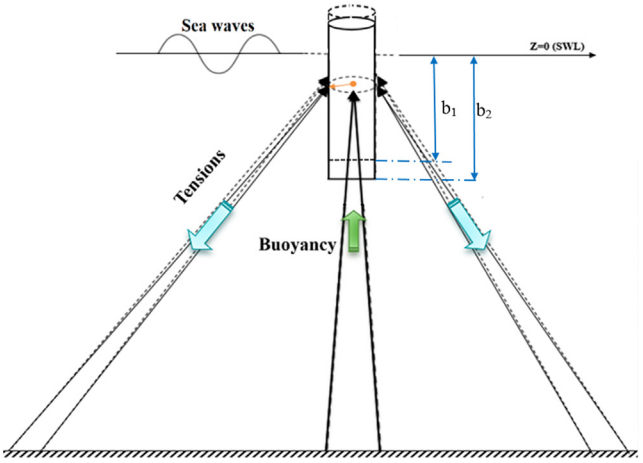

Fig. 4 An example of 6–6 FPMR shows the effect of the weight on the submerged depth and the cable tensions.

$$K = \frac{dF}{dX} = K_k + K_\tau \tag{3}$$

$$K_k = \sum_{i=1}^{6} k_i \begin{bmatrix} \hat{s}_i\hat{s}_i^T & \hat{s}_i\hat{s}_i^T[b_iX]^T \\ [b_iX]\hat{s}_i\hat{s}_i^T & [b_iX]\hat{s}_i\hat{s}_i^T[b_iX]^T \end{bmatrix} \tag{4}$$

$$K_\tau = \sum_{i=1}^{6} \frac{T_i}{l_i} \begin{bmatrix} I - \hat{s}_i \hat{s}_i^T & (I - \hat{s}_i \hat{s}_i^T)[b_i X]^T \\ [b_i X](I - \hat{s}_i \hat{s}_i^T) & [b_i X](I - \hat{s}_i \hat{s}_i^T)[b_i X]^T - l_i[\hat{s}_i X][b_i X] \end{bmatrix} \tag{5}$$

where $\mathbf{I}$ is the identity matrix; l_i is the i_{th} cable-bundle length; k_i is the i_{th} cable-bundle material stiffness; $\hat{\boldsymbol{s}}_i$ is the unit vectors in the direction of the cable-bundles; and $[\hat{\boldsymbol{s}}_i \boldsymbol{X}]$ and $[\boldsymbol{b}_i \boldsymbol{X}]$ are matrices which are represented by Eq. (6).

$$[\hat{s}_i X] = \begin{bmatrix} 0 & -\hat{s}_{iz} & \hat{s}_{iy} \\ \hat{s}_{iz} & 0 & -\hat{s}_{ix} \\ -\hat{s}_{iy} & \hat{s}_{ix} & 0 \end{bmatrix}, [b_i X] = \begin{bmatrix} 0 & -b_{iz} & b_{iy} \\ b_{iz} & 0 & -b_{ix} \\ -b_{iy} & b_{ix} & 0 \end{bmatrix} \tag{6}$$

The hydrostatic stiffness occurs due to the change in the center of buoyancy (CB) which arises from the motion of the floating structure in the heave, roll and pitch directions [17,38,39]. Therefore, an added stiffness matrix can be written as:

$$K_a = \begin{bmatrix} 0 & 0 & 0 & 0 & 0 & 0 \\ 0 & 0 & 0 & 0 & 0 & 0 \\ 0 & 0 & k_{a33} & 0 & 0 & 0 \\ 0 & 0 & 0 & k_{a44} & 0 & 0 \\ 0 & 0 & 0 & 0 & k_{a55} & 0 \\ 0 & 0 & 0 & 0 & 0 & 0 \end{bmatrix} \tag{7}$$

where $k_{a33} = \rho_f g A_s$, $k_{a44} = k_{a55} = \rho_f g A_s D\left(\bar{KG} - \bar{KB}\right)$, and $A_s = \frac{\pi}{4} D^2$. $D = 2r$ which represents the diameter of the floating structure, g is the gravitational acceleration, and $\bar{KB}$ is the distance between the SWL and the CB.

The stiffness matrix has translational and rotational values with differences in the physical units. Hence, natural frequencies of the FPMR are used to evaluate its stiffness in different conditions and locations. The natural frequencies of the FPMR have a common physical unit (Hz) and it is used as an indicator of the FPMR stiffness. Considering the cable-bundles as springs, the FPMR natural frequencies are computed using [19,40].

$$f_j^k = \frac{\sqrt{eig_j\left(M^{-1}M^k\right)}}{2\pi} \tag{8}$$

where f_j^k is the j^{th} FPMR natural frequency at the k^{th} pose/location (in Hz) $eig_j(matrix)$; represents the j^{th} eigenvalue of the matrix; $\boldsymbol{K^k}$ is the FPMR stiffness matrix at the k^{th} pose/location.

Using the modal analysis method [41], Eq. (1) can be changed to the uncoupled differential equation form as given below:

$$\boldsymbol{X}_i(t) = \boldsymbol{U}\boldsymbol{Q}_i(t) \tag{9}$$

$$\boldsymbol{M}(X)\boldsymbol{U}\ddot{\boldsymbol{Q}} + \boldsymbol{K}\boldsymbol{U}\boldsymbol{Q} = \boldsymbol{F}(t, X) \tag{10}$$

$$\boldsymbol{U}^T\boldsymbol{M}(X)\boldsymbol{U}\ddot{\boldsymbol{Q}} + \boldsymbol{U}^T\boldsymbol{K}\boldsymbol{U}\boldsymbol{Q} = \boldsymbol{U}^T\boldsymbol{F}(t, X) \tag{11}$$

$$\ddot{\boldsymbol{Q}}_i(t) + \omega_i^2 \boldsymbol{Q}_i(t) = \boldsymbol{N}_i(t),\ \boldsymbol{N}_i(t) = \boldsymbol{U}^T\boldsymbol{F}(t, X) \tag{12}$$

Where $\boldsymbol{X_i(t)}$ represents the generalized coordinates, $\boldsymbol{U}$ is the shape vectors matrix (modal matrix), $\boldsymbol{Q_i}(t)$ represents the natural coordinates, and ω_i represents the FPMR natural frequencies.

$$\boldsymbol{Q}_i(t) = \frac{1}{\omega_i} \int_0^t \boldsymbol{N}_i(\tau) sin\omega_i(t-\tau)d\tau, i = 1, 2, \cdots, 6 \tag{13}$$

Eq. (13) gives the solution of Eq. (12) where.$\boldsymbol{X}_i(t) = \boldsymbol{U}\boldsymbol{Q}_i(t)$

Positive cable-bundles' tensions are required to avoid negative tensions in the cable-bundles. Eq. (14) is used to calculate the cable-bundles' tensions.

$$T_i = k\Delta L_i, i = 1, \cdots., 6 \tag{14}$$

Where k represents the cable-bundles' stiffness, and ΔL is the change in the cable-bundles' length.

4. Methodology

The current study deals with studying the effect of changing cables' patterns on the workspace of six DOFs FPMR. To evaluate the effect of the changing cables' pattern, two FPMR cable-bundles' configurations i.e., 6–6 Stewart-Gough parallel manipulator configuration and a new cable-bundles' configuration called 6–3-3 FPMR were compared in this study. In both configurations, the FPMR was subjected to the external forces generated by the sea waves. Six DOFs FPMR with twelve cables (6 bundles) was used in this study. Then, the enhancement in the workspace and the dynamic behavior of the FPMR were calculated. The flow chart shown in Fig. 5 represents the calculation scheme while analyzing this section. The area borders in which the platform will work, the initial platform location, and the submerged depth were first specified, followed by calculating the mass and stiffness matrices using Eqs. (2) and (3). Eqs. (8) and (13) were then used to find the natural frequency and dynamic response. Based on Eq. (14), the location that is included in the workspace was calculated along with the corresponding natural frequency and dynamic behavior.

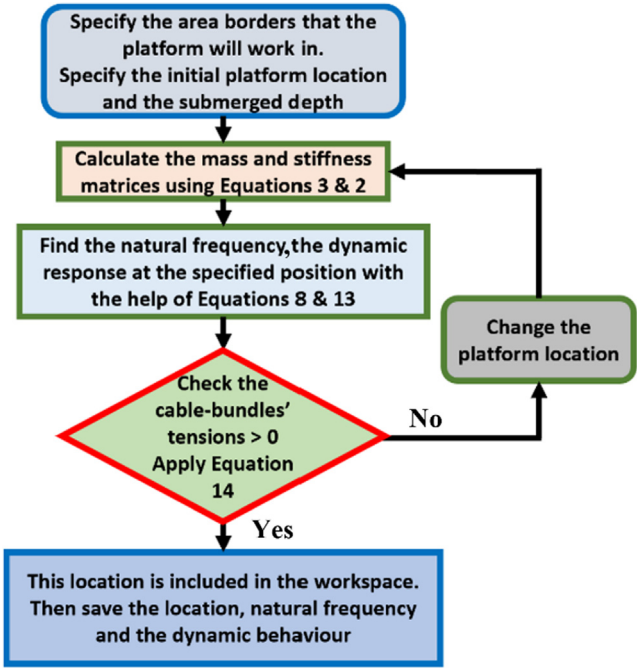

Fig. 5 Flow chart of the methodology followed in the current study.

5. Results and discussion

Two case studies are performed in this section. The first case is without the hydrostatic effect and the second case is with the hydrostatic effect. To compare between 6 and 6 and 6–3-3 FPMR configurations, the dynamic response is analyzed for the same pose/location of $X = 50m$, $Y = 30m$, and depth of the submerged part of the structure $b = 0.8m$. The results shown in Figs. 6 and 7, which show the dynamic response in different DOFs, i.e., surge, sway, heave, roll, pitch, and yaw. These results show that the average displacement and rotational amplitudes of all DOFs in the 6–3-3 configuration are lower than in the 6–6 configuration, which means higher relative stability in the 6–3-3 FPMR configuration than in the 6–6 FPMR configuration. At the same time, it is clear in the responses that the hydrostatic effect helps in decreasing the displacement and rotational responses' amplitudes and in all DOFs. However, the effect is clearer in surge and heave directions. Based on Figs. 6 and 7, the 6–3-3 FPMR configuration is more stable when compared to the 6–6 configuration, and considering the hydrostatic effect further increases the stability. As shown in Fig. 8, the workspace of the 6–3-3 configuration is also large as compared to the 6–6 configuration.

Fig. 9 shows the minimum natural frequencies of the FPMR, within the same workspaces that are shown in Fig. 8. In general, the 6–3-3 FPMR has a larger minimum natural frequency in all FPMR poses/locations. A larger minimum natural frequency indicates that the platform is more rigid and has more stability. This complements the 6–3-3 configuration and allows it to be preferred on the 6–6 configuration concerning stability. This increase in stability will be helpful to use the 6–3-3 FPMR configuration in the sea environment conditions more safely than the 6–6 FPMR configuration. It is clearly shown that the stiffness of the 6–3-3 FPMR has a higher magnitude than that of the 6–6 FPMR.

The cable-bundles' directions control the directions of the internal forces of the cable-bundles and therefore the cable-bundles' layout has an evident effect on the FPMR workspace. The internal forces in the 6–3-3 FPMR configuration are stronger than the 6–6 FPMR configuration to compensate for the environmental loads in a larger workspace and protect the FPMP from cable-bundles' slack or failure (i.e. negative

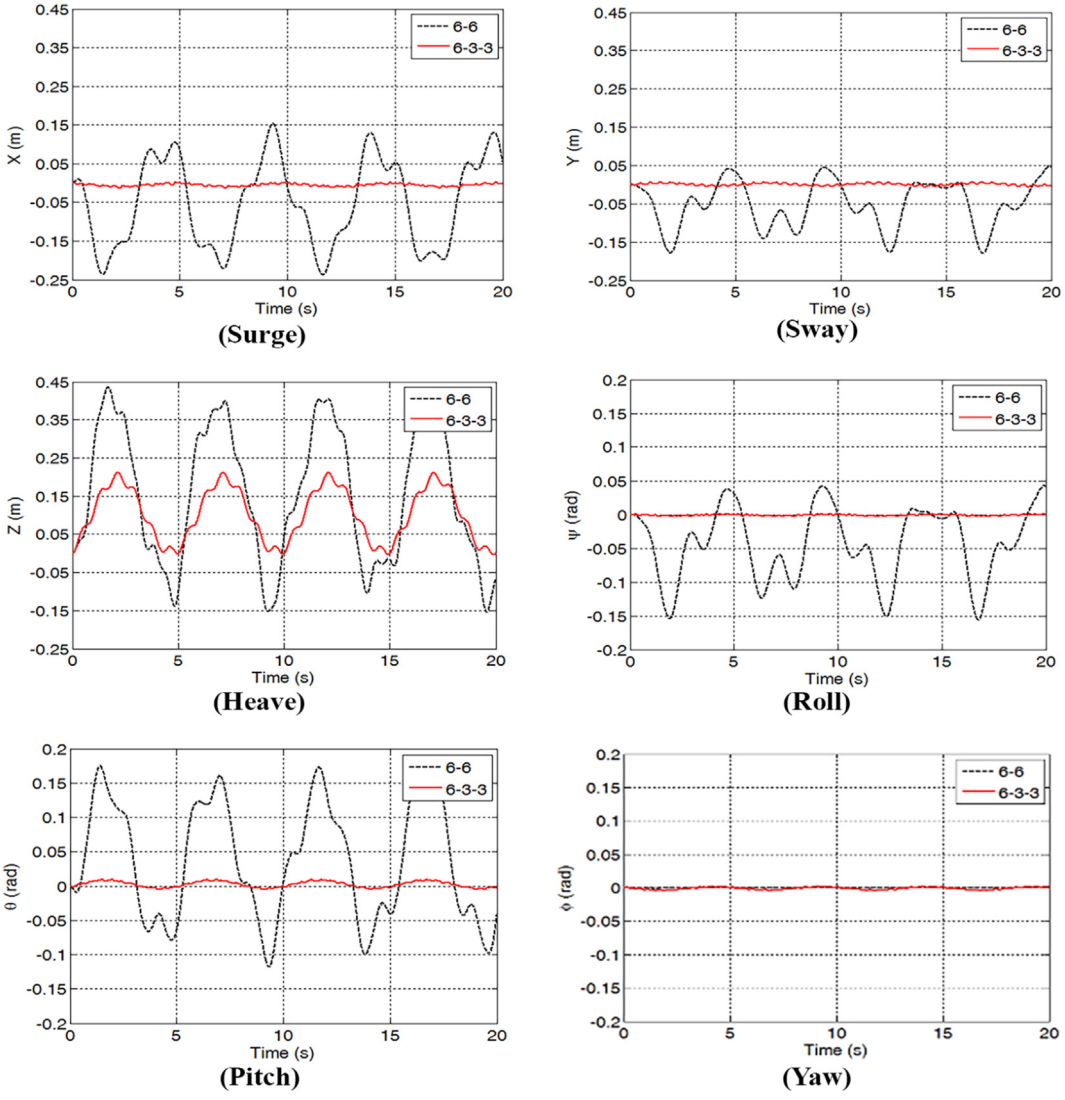

Fig. 6 6–3-3, and 6–6 FPMR dynamical responses considering case 1.

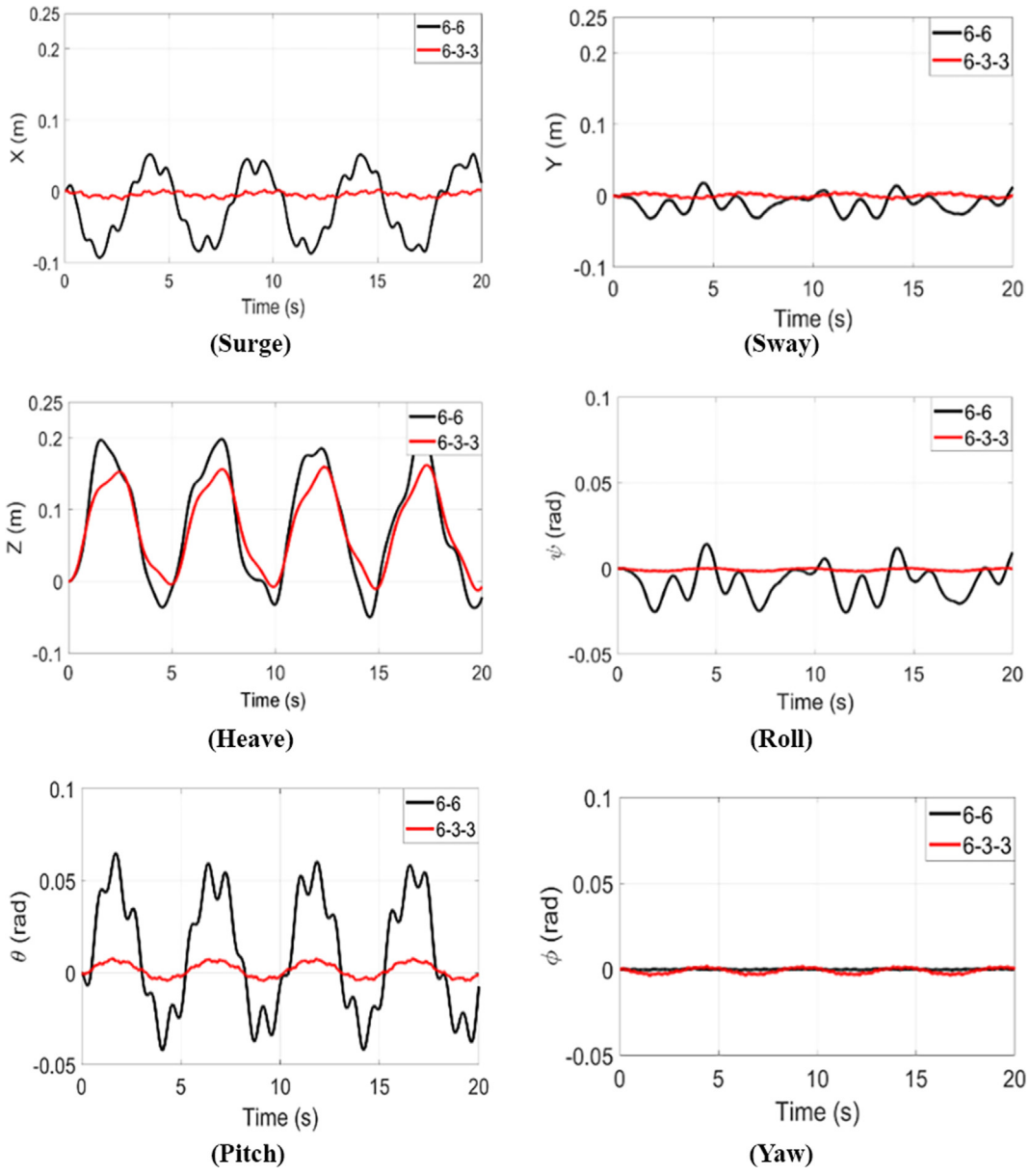

Fig. 7 6–3-3, and 6–6 FPMR dynamical responses considering case 2.

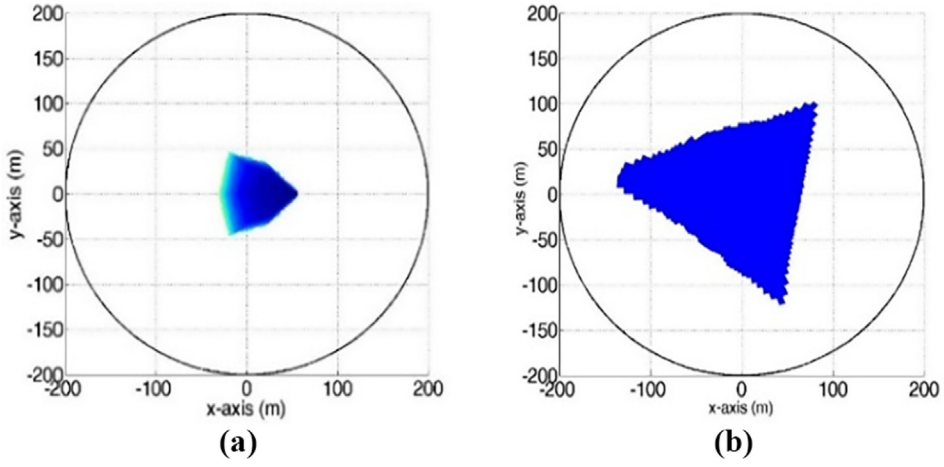

Fig. 8 Workspaces of the FPMR (a) 6–6 configuration (b) 6–3-3 configuration.

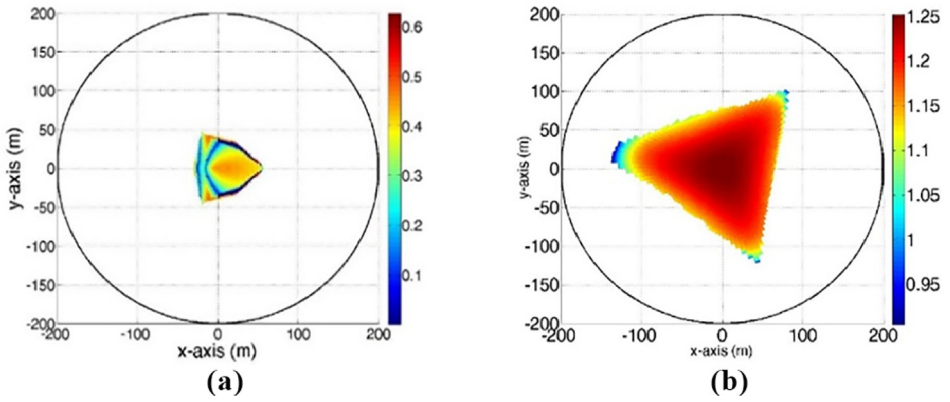

Fig. 9 Minimum Frequencies (color, Hz) within the FPMR workspaces shown in Fig. 4 (a) 6–6 configuration (b) 6–3-3 configuration.

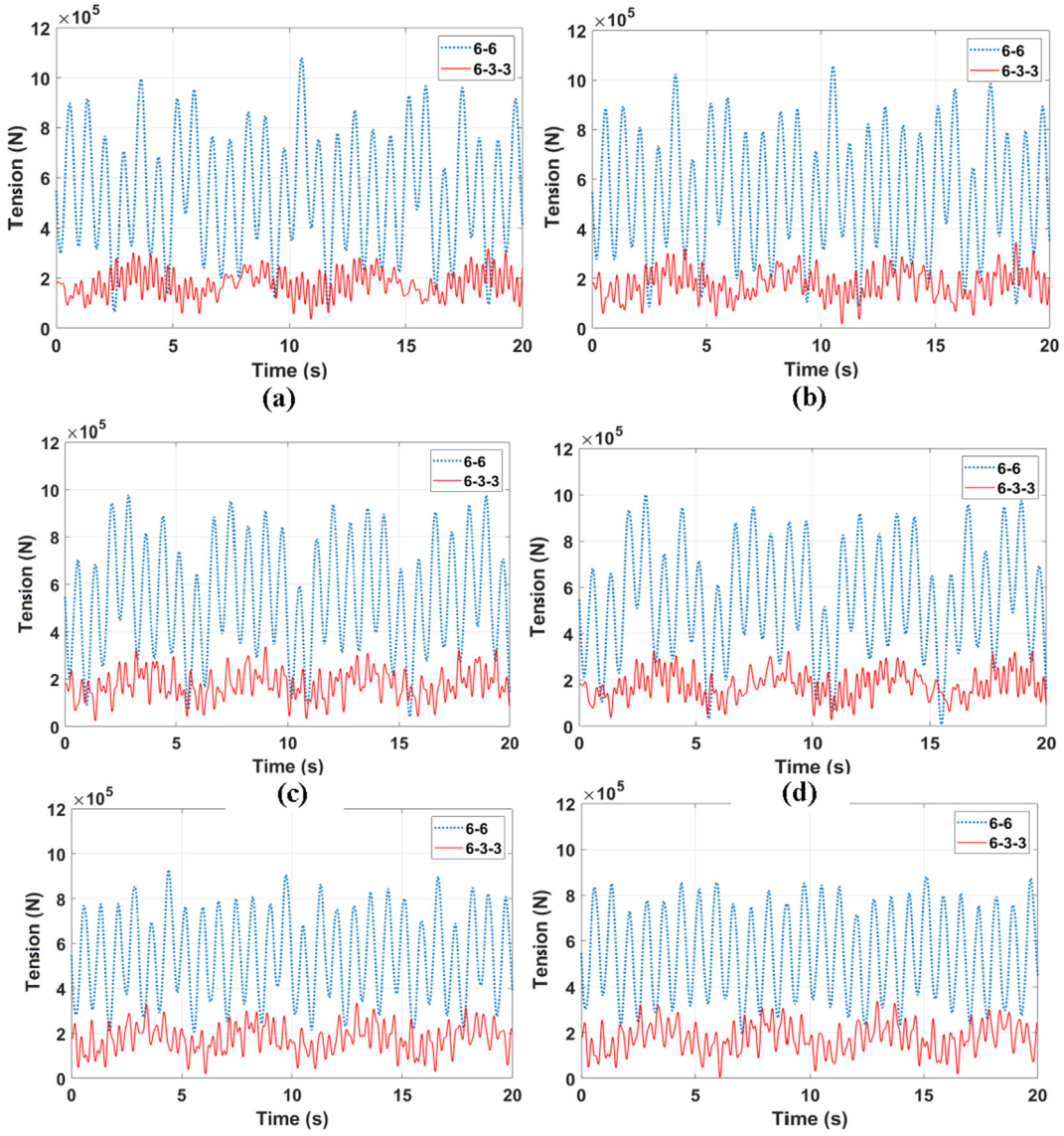

Fig. 10 Cables tensions at pose/location where $\boldsymbol{X} = 10\boldsymbol{m}$, and $\boldsymbol{Y} = 10\boldsymbol{m}$ (a) Cable 1 (b) Cable 2 (c) Cable 3 (d) Cable 4 (e) Cable 5 (f) Cable 6.

Table 2 The RMS values of the cable-bundles tensions at pose $X = 10\,m$, and $Y = 10\,m$.

Configurations	Cable 1 (N)	Cable 2 (N)	Cable 3 (N)	Cable 4 (N)	Cable 5 (N)	Cable 6 (N)
6–6 (b = 1.21 m)	$5.93 * 10^5$	$5.94 * 10^5$	$5.91 * 10^5$	$5.92 * 10^5$	$5.76 * 10^5$	$5.77 * 10^5$
6–3-3 (b = 0.73 m)	$1.84 * 10^5$	$1.86 * 10^5$	$1.87 * 10^5$	$1.87 * 10^5$	$1.88 * 10^5$	$1.89 * 10^5$

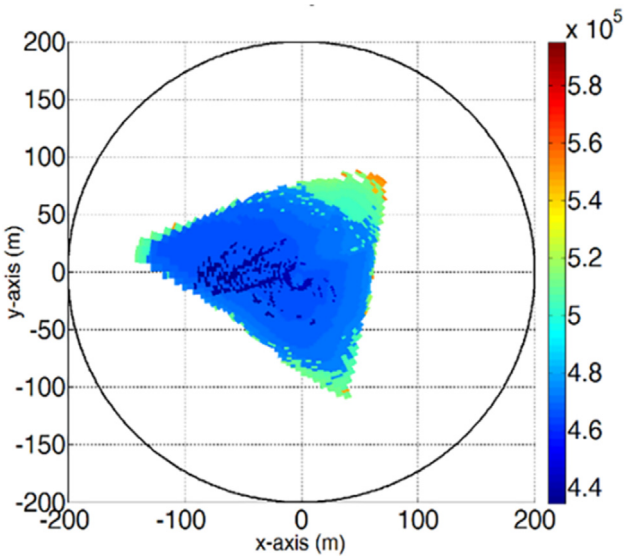

Fig. 11 The 2nd-norm value of the cable tensions at each pose/location in the 6–3-3 FPMR workspace (N/m).

cable-bundles' tensions). So, it is crucial to study the effect of the new proposed configuration (6–3-3 FPMR) on the cable-bundles' tensions.

The cable-bundles' tensions of the 6–6 and 6–3-3 FPMR configuration are investigated in the same pose with the same submerged depth. The selected pose is at $X = 10\,m$, and $Y = 10\,m$ which is chosen to be within the two configurations workspaces. The minimum submerged depth, at the selected pose, that is needed to avoid the cable-bundles slack is 1.21 m for 6–6 configuration and 0.73 m for 6–3-3 configuration respectively. Fig. 10 shows the cable-bundles' tensions for the two configurations at the mentioned pose. It is observed that the tensions are positive inside all cable-bundles' for the two configurations but the 6–3-3 configuration requires cable-bundles' tensions less than 6–6 configuration to compensate for the environmental loads. While 6–3-3 configuration, at submerged depth equal to 0.73 m, has a 2nd norm value for all cable-bundles tensions equal to $4.5724 * 10^5$ N, the 6–6 configuration, at submerged depth equal to 1.21 m, has a 2nd norm value for all cable-bundles tensions equal to $1.4389 * 10^6$, see Table 2. Hence, it is concluded that the 6–3-3 configuration needs lower submerged depth and less cable-bundles tensions to avoid cable-bundles failure and to compensate for the environmental loads.

The second norm of the root means square (RMS), values of the cable-bundles' tensions are shown in Fig. 11. High cable-bundles' tensions are needed to keep all cable-bundles taut, as the floating structure is becoming closer to the workspace borderline. The RMS values of the linear and rotational displacements within the workspace are presented in Fig. 12. It is observed that higher RMS displacements values are achieved in the third DOF (heave motion) compared with the surge and sway motions. Higher RMS rotational displacements values occurred at all of the FPMR workspace edges. The colored areas in Fig. 12 represent the workspaces of the platforms that can work while keeping all cable-bundles taut.

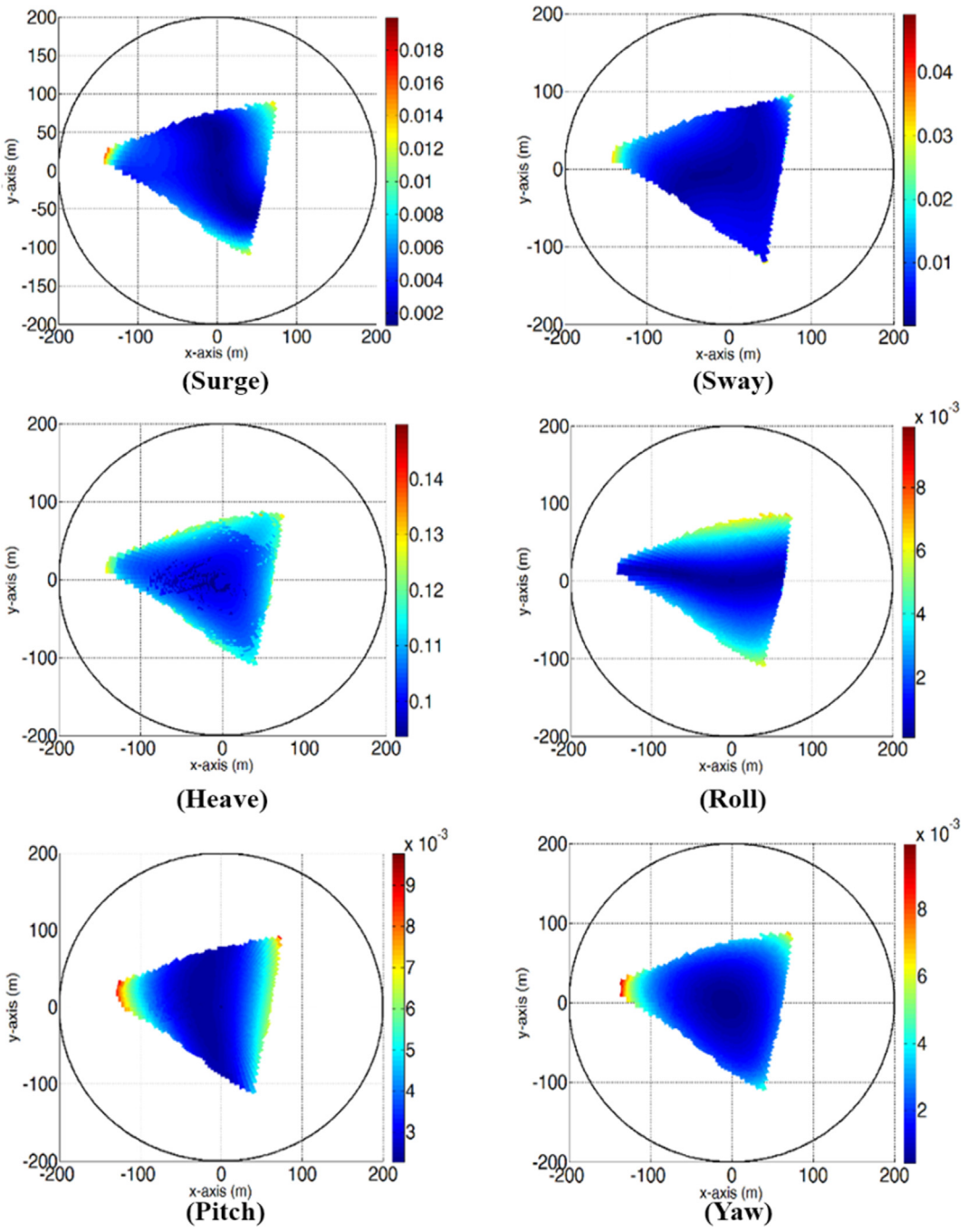

Fig. 12 6–3-3 FPMR dynamical responses within its workspace, color is in [m] for the linear displacement and in radian for rotational displacement.

6. Conclusion

An FPMR was presented in the current study, such that the floating structure moves on a certain sea surface (i.e., workspace). The workspace, mass, stiffness, forces equations, and dynamic behavior for the FPMR were investigated. The dynamical response analysis was evaluated on the sea surface in a certain location for two cases, which are with and without the hydrostatic effect. The outcomes of the current study are summarized as follows:

- The 6–3-3 FPMR configuration is more stable as compared to the 6–6 configuration and considering the hydrostatic effect increases the stability of both configurations.
- The workspace of the 6–3-3 configuration is large as compared to the 6–6 configuration.
- In general, the 6–3-3 FPMR has a larger minimum natural frequency in all FPMR poses/locations. A larger minimum natural frequency indicates that the platform is more rigid and has more stability. This complements the 6–3-3 configuration and allows it to be preferred on the 6–6 configuration with regard to stability. This increase the stability and

it will be helpful to use the 6–3-3 FPMR configuration in the sea environment conditions more safely than the 6–6 FPMR configuration.

- The stiffness of 6–3-3 FPMR has a higher magnitude than that of the 6–6 FPMR. The cable-bundles' directions control the directions of the internal forces of the cable-bundles and therefore the cable-bundles' layout has an evident effect on the FPMR workspace. The internal forces in the 6–3-3 FPMR configuration are stronger to compensate for the environmental loads in a larger workspace and protect the FPMP from cable-bundles' slack or failure (i.e. negative cable-bundles' tensions).
- High cable-bundles' tensions are needed to keep all cable-bundles taut, as the floating structure is becoming closer to the workspace borderline. It is observed that higher RMS displacements values are achieved in the third DOF (heave motion) compared with the surge and sway motions.
- After All, it can be concluded that the 6–3-3 FPMR is more rigid/stable and secure in the marine environment as compared to the 6–6 FPMR.

Declaration of Competing Interest

The authors declare that they have no known competing financial interests or personal relationships that could have appeared to influence the work reported in this paper.

Acknowledgments

The authors acknowledge their Universities (Birzeit University, Hebron University, King Fahd University of Petroleum and Minerals (KFUPM), and Imam Abdulrahman bin Faisal University).

Appendix A. The following analytical expressions represents the water wave excitation forces on the floating vertical cylindrical disk [19,37]:

$$F_j = \widehat{F}_j \, \mathrm{e}^{-i\omega t}, j = x, z and T \tag{16}$$

$$\widehat{F}_x = -\frac{\pi i \rho_f g H r}{k_o}\left(\mathrm{J}_1(k_o r) - \frac{\mathrm{J}_1'(k_o r)}{\mathrm{H}_1'(k_o r)}\mathrm{H}_1(k_o r)\right)\left(1 - \mathrm{e}^{-k_o b}\right)$$

$$\widehat{F}_z = 2\pi i \rho_f \omega r \sqrt{\frac{2}{\pi}} \int_0^{\infty} \mathrm{P}_0(\xi) \frac{\mathrm{I}_1(\xi r)}{\xi \mathrm{I}_0(\xi r)} d\xi$$

$$\begin{aligned}\widehat{F}_T &= M_y \\ &= \pi i \rho_f g H r \left(\mathrm{J}_1(k_o r) - \frac{\mathrm{J}_1'(k_o r)}{\mathrm{H}_1'(k_o r)}\mathrm{H}_1(k_o r)\right) \int_0^b (z-b) e^{-k_o z} dz \\ &\quad - \pi i \rho_f \omega r^2 \sqrt{\frac{2}{\pi}} \int_0^{\infty} \mathrm{P}_1(\xi) \frac{\mathrm{I}_2(\xi r)}{\xi \mathrm{I}_1(\xi r)} d\xi\end{aligned}$$

where J_m denotes a Bessel function of the first kind of order m, I_m denotes a modified Bessel function of the first kind of order m, H_m is the Hankel function of the first kind of order m, primes denote differentiation with respect to arguments, ω is the water wave frequency, k_0 is the wavenumber, $k_0 = \frac{2\pi}{\lambda}$ and λ is the wavelength. H is the peak-to-peak wave height, ϵ_m is Neumann's number, $\epsilon_o = 1, \epsilon_m = 2, m \geq 1$, and $\mathrm{P}_m(\xi) = -\frac{gH}{2\omega}\epsilon_m i^{m+1}\sqrt{\frac{2}{\pi}} * \left(\mathrm{J}_m(k_o r) - \frac{\mathrm{J}_m'(k_o r)}{\mathrm{H}_m'(k_o r)}\mathrm{H}_m(k_o r)\right)\frac{\mathrm{e}^{-k_o b}k_\theta}{\xi^2 + k_o^2}$.

References

[1] P.H. Borgstrom, N.P. Borgstrom, M.J. Stealey, B. Jordan, S. Gaurav, M.A. Batalin, et al, Discrete trajectory control algorithms for NIMS3D, an autonomous underconstrained three-dimensional cabled robot, IEEE/RSJ Int. Conf. Intell. Robots Syst. 2007 (2007) 253–260.

[2] J. Albus, R. Bostelman, N. Dagalakis, The NIST robocrane, J. Robot. Syst. 10 (5) (1993) 709–724.

[3] S. Kawamura, W. Choe, S. Tanaka, S.R. Pandian, Development of an ultrahigh speed robot FALCON using wire drive system, in: Proceedings of 1995 IEEE International Conference on Robotics and Automation, 1995, pp. 215-220 vol.1.

[4] K. Maeda, S. Tadokoro, T. Takamori, M. Hiller, R. Verhoeven, On design of a redundant wire-driven parallel robot WARP manipulator, in: Proceedings 1999 IEEE International Conference on Robotics and Automation (Cat. No.99CH36288C), 1999, pp. 895-900 vol.2.

[5] C. Ferraresi, M. Paoloni, S. Pastorelli, F. Pescarmona, A new 6-DOF parallel robotic structure actuated by wires: the WiRo-6.3, J. Robot. Syst. 21 (11) (2004) 581–595.

[6] S. Behzadipour, A. Khajepour, A new cable-based parallel robot with three degrees of freedom, Multibody Sys.Dyn. 13 (4) (2005) 371–383.

[7] G. Mroz, L. Notash, Design and prototype of parallel, wire-actuated robots with a constraining linkage, J. Robot. Syst. 21 (12) (2004) 677–687.

[8] S.A. Maffra, Genetic Algorithm Optimization for Mooring Systems, 2001

[9] E. Ueland, T. Sauder, R. Skjetne, Optimal force allocation for overconstrained cable-driven parallel robots: continuously differentiable solutions with assessment of computational efficiency, IEEE Trans. Rob. 37 (2) (2020) 659–666.

[10] D. Gueners, B.-C. Bouzgarrou, H. Chanal, Cable behavior influence on cable-driven parallel robots vibrations: experimental characterization and simulation, J. Mech. Robot. 13 (4) (2021).

[11] I. Chawla, P.M. Pathak, L. Notash, A.K. Samantaray, Q. Li, U. K. Sharma, Effect of selection criterion on the kineto-static solution of a redundant cable-driven parallel robot considering cable mass and elasticity, Mech. Mach. Theory 156 (2021) 104175.

[12] H. Hussein, J. Santos, J. Izard, M. Gouttefarde, Smallest maximum cable tension determination for cable-driven parallel robots, IEEE Trans. Rob. 37 (4) (2021) 1186–1205.

[13] M.R. Mousavi, M. Ghanbari, S.A.A. Moosavian, P. Zarafshan, Rapid and safe wire tension distribution scheme for redundant cable-driven parallel manipulators, Robotica 40 (7) (2022) 2395–2408.

[14] L. Tang, M. Gouttefarde, A. Doria, H. Sun, H. Wang, C. Zhou, Analysis and verification of cable pretension effect on the buckling load of a single-link flexible mechanism, Appl. Math. Model. 104 (2022) 499–516.

[15] M. Shafieefar, A. Rezvani, Mooring optimization of floating platforms using a genetic algorithm, Ocean Eng. 34 (2007/07/01/ 2007.) 1413–1421.

[16] B.d.F. Monteiro, C.H. Albrecht, B.P. Jacob, Application of the Particle Swarm Optimization Method on the Optimization of Mooring Systems for Offshore Oil Exploitation, 2010.

[17] O.A. Montasir, A. Yenduri, V.J. Kurian, Effect of mooring line configurations on the dynamic responses of truss spar platforms, Ocean Eng. 96 (2015/03/01/ 2015.) 161–172.
[18] I. Felix-Gonzalez, R.S. Mercier, Optimized design of statically equivalent mooring systems, Ocean Eng. 111 (2016/01/01/ 2016.) 384–397.
[19] M.M. Horoub, S. Khan, S. Ali, A.M. Horoub, Comparative Analysis of a Floating Mooring Line-Driven Platform (FMDP) Having Different Mooring Lines Patterns, in: 2018 9th International Conference on Mechanical and Aerospace Engineering (ICMAE), 2018, pp. 269-273.
[20] S. Kawamura, K. Ito, A new type of master robot for teleoperation using a radial wire drive system, in: Proceedings of 1993 IEEE/RSJ International Conference on Intelligent Robots and Systems (IROS '93), 1993, pp. 55-60 vol.1.
[21] A. Ming, T. Higuchi, Study on multiple degree-of-freedom positioning mechanism using wires. I: Concept, design and control, Int. J. Jpn Soc. Precis. Eng. 28 (1994) 131–138.
[22] R.G. Roberts, T. Graham, T. Lippitt, On the inverse kinematics, statics, and fault tolerance of cable-suspended robots, J. Robot. Syst. 15 (10) (1998) 581–597.
[23] J. Pusey, A. Fattah, S. Agrawal, E. Messina, Design and workspace analysis of a 6–6 cable-suspended parallel robot, Mech. Mach. Theory 39 (7) (2004) 761–778.
[24] E. Stump, V. Kumar, Workspaces of Cable-Actuated Parallel Manipulators, J. Mech. Des. 128 (2005) 159–167.
[25] C.B. Pham, S.H. Yeo, G. Yang, M.S. Kurbanhusen, I.-M. Chen, Force-closure workspace analysis of cable-driven parallel mechanisms, Mech. Mach. Theory 41 (1) (2006) 53–69.
[26] P. Bosscher, A.T. Riechel, I. Ebert-Uphoff, Wrench-feasible workspace generation for cable-driven robots, IEEE Trans. Rob. 22 (5) (2006) 890–902.
[27] M. Gouttefarde, C.M. Gosselin, Analysis of the wrench-closure workspace of planar parallel cable-driven mechanisms, IEEE Trans. Rob. 22 (3) (2006) 434–445.
[28] D. Xiumin, M. Ou, "Force-closure analysis of general 6-DOF cable manipulators, IEEE/RSJ Int. Conf. Intell. Robots Syst. 2007 (2007) 3931–3936.
[29] S. Behzadipour, A. Khajepour, Stiffness of cable-based parallel manipulators with application to stability analysis, J. Mech. Des. 128 (2005) 303–310.
[30] M.H.A. Ghaffar, Study on Cable Based Parallel Manipulator Systems for Subsea Applications, in: Proceedings of the 3rd International Conference on Mechanical Engineering and Mechatronics,, Prague, Czech Republic, 2014, pp. 1-8.
[31] A. Ghaffar, M. Hassan, Failure Analysis of Cable Based Parallel Manipulators, Appl. Mech. Mater. 736 (2015) 203–210.
[32] M.M. Horoub, Dynamic Analysis of a Tension Leg Platforms (TLPs) Inspired by Parallel Robotic Manipulators, IEEE Access 8 (2020) 35222–35230.
[33] L.W. Tsai, Robot analysis: the mechanics of serial and parallel ma-nipulators, 1999.
[34] F. Ferreira, G. Ferri, Marine robotics competitions: a survey, Curr. Robot. Rep. 1 (2020) 169–178.
[35] E. Zereik, M. Bibuli, N. Mišković, P. Ridao, A. Pascoal, Challenges and future trends in marine robotics, Annu. Rev. Control 46 (2018.) 350–368.
[36] R. G. Vincenzo Parenti-Castelli, Closed-form solution of the direct kinematics of the 6–3 type Stewart Platform using one extra sensor, in: Meccanica (Ed.)vol. 31, 1996, p. 10.
[37] W. Finnegan, M. Meere, J. Goggins, The wave excitation forces on a truncated vertical cylinder in water of infinite depth, J. Fluids Struct. 40 (2013/07/01/ 2013.) 201–213.
[38] R. Mansouri, H. Hadidi, Comprehensive study on the linear hydrodynamic analysis of a truss spar in random waves, World Acad. Sci. Eng. Technol. 53 (2009) 01/01.
[39] A.K. Agarwal, A.K. Jain, Nonlinear coupled dynamic response of offshore Spar platforms under regular sea waves, Ocean Eng. 30 (2003.) 517–551.
[40] M. Hassan, A. Khajepour, Analysis of a large-workspace cable-actuated manipulator for warehousing applications, in: ASME 2009 International Design Engineering Technical Conferences and Computers and Information in Engineering Conference, 2009, pp. 45-53.
[41] P. Lengvarský, J. Bocko, Theoretical Basis of Modal Analysis, Am. J. Mech. Eng. 1 (2013) 173–179.